PAPER

Check for updates

Designing a micro-cellulose membrane for hydrogen fuel cells†

Aniket Raut,‡[a] Haoyan Fang, [ID] ‡[a] Yu-Chung Lin,[a] Md Farabi Rahman,[a] Shi Fu,[a] Yifan Yin,[a] Yiwei Fang,[a] David Sprouster, [ID] [a] Rebecca Isseroff,[a] Sunil K. Sharma, [ID] [a] Priyanka Sharma,[b] Devanshi Bhardwaj,[a] Mounesha N. Garega,[c] Steve Greenbaum,[c] Sheng Zhang[d] and Miriam Rafailovich [ID] *[a]

In this paper we describe the use of micro-cellulose, as obtained directly from cellulose filter paper, treated with weak acids, and reinforced with resorcinol bis(diphenyl phosphate) (RDP), for incorporation into the Membrane Electrolyte Assembly (MEA) of proton exchange membrane fuel cells (PEMFCs). The addition of RDP created a film on the cellulose fibers, preventing gas crossover and improving proton dynamics. FTIR analysis showed RDP binding to cellulose hydroxyl groups *via* the phenolic segments, while citric and phosphoric acids hydrolyzed the cellulose, causing RDP to bind *via* the P–O site. NMR analysis confirmed strong hydrogen bonding between RDP and cellulose, resulting in low proton mobility. However, RDP introduced after acid treatment, and binding at the P–O site, significantly enhanced proton mobility. Testing MEAs with RDP-treated cellulose filter membranes achieved a maximum power output of 4.9 mW cm^{-2} at 80 °C with only 0.1 mg cm^{-2} of platinum group metal loading. Treatment with citric or phosphoric acid increased power output by 141% and 120%, respectively, reaching a peak at 60 °C. The highest power output (16 mW cm^{-2} in air, 34.3 mW cm^{-2} in oxygen) was achieved with a mixed acid-treated membrane, displaying an ion exchange capacity of 0.1 m$_{eq.}$ g^{-1} and 226% power enhancement. The membrane remained stable at 60 mA for 100 hours, with an 8% voltage loss. This work shows that cellulose filter paper, which requires minimal additional processing and is easily recycled, can provide a cost-effective, environmentally sustainable choice for low power PEMFC applications.

Sustainability spotlight

Hydrogen fuel cells offer a clean alternative for energy generation, producing only water as a byproduct. While most research has concentrated on high-current applications such as transportation or power grids, portable or personal electronics, which require significantly lower voltages, represent a more common use case. Traditional chemical batteries in such devices often have shorter lifespans and create environmental challenges when discarded. In this study, we propose a sustainable alternative: hydrogen fuel cells incorporating an inexpensive cellulose membrane for these low-voltage applications. These cells are both safe to dispose of and fully recyclable. By lowering the cost of portable electronics, this approach can make them more accessible to economically disadvantaged communities while minimizing environmental impact.

1. Introduction

The need to address rising global energy consumption and environmental pollution brought on using fossil fuels has sparked an increase in the use of renewable and environmentally friendly energy sources worldwide.[1–10] A hydrogen economy based on renewable energy sources including hydrogen generation, hydrogen storage, and hydrogen power conversion is widely seen as a possible energy future option.[11–16] Due to their high efficiency and low emissions, PEM (Polymer Electrolyte Membrane) fuel cell technologies have attracted attention from all over the world. Polymer electrolyte membranes, particularly Nafion®, are used in the construction of PEM fuel cells as the proton conductor and as the electrochemical catalyst for electrochemical processes occurring at low temperatures. PEM fuel cells are a strong choice for the next generation of power sources for transportation, stationery, and portable applications due to their notable characteristics of low operating temperature, high power density, sustainable and recyclable

[a]*Department of Materials Science and Chemical Engineering, State University of New York at Stony Brook, New York 11794, USA. E-mail: miriam.rafailovich@stonybrook.edu*

[b]*Department of Chemical and Paper Engineering, Western Michigan University, Kalamazoo, Michigan 49008, USA*

[c]*Department of Physics & Astronomy, Hunter College of the City University of New York, 695 Park Ave, New York, NY 10065, USA*

[d]*The Advanced Science Research Center, Graduate Center of the City University of New York, 85 St. Nicholas Terrace, New York, New York 10031, USA*

† Electronic supplementary information (ESI) available. See DOI: https://doi.org/10.1039/d4su00728j

‡ These authors contributed equally to this work.

potential[17,18] and simple scale-up.[19–25] But their high cost impedes the widespread commercialization of the technology. The cost of the Nafion membranes and the platinum group metal catalyst contribute to the high cost. A great deal of effort has been invested in finding alternatives.[11–14,26–31]

Cellulose is a natural polysaccharide contained in biomass and is the most abundant biopolymer on the planet.[32–35] Compared to the global reserves of fossil fuels, our biosphere generates more than 1.5×10^{15} kg of cellulose annually.[36,37] Cellulose is a simple linear polymer comprised of glucose units bound together via 1,4 β-glycosidic bonds. The long polymer chains of cellulose bind together via intra and intermolecular hydrogen bonding to form microfibrils due to the presence of reactive hydroxyl groups in its chemical structure.[38] Because of the strong intra- and inter-molecular hydrogen bonding network, it exhibits high mechanical strength and is also potentially useful for proton conduction.[39,40] Microcrystalline cellulose was first investigated in 2009,[41] when a succession of crosslinked polymer electrolyte membranes for fuel cell applications was reported, by blending cellulose and sulfosuccinic acid (SA) via esterification reaction. More recently, a comprehensive review summarized the performance and composition of a whole range of materials used for PEM fuel cell membranes, where different forms of cellulose, many with additional functionalizing, comprised the majority of the biomaterials used.[42] Crystalline nanocellulose was incorporated into an MEA which produced a maximum power output of 17.2 mW cm^{-2} at 80 °C and 95% relative humidity (RH).[43] Songtao et al. synthesized citric acid cross-linked cellulose nano fiber (CNF) membranes which exhibited the maximum power density of 27.7 mW cm^{-2} in oxygen environment at 80 °C and 100% relative humidity (RH) with 0.1 mg cm^{-2} Pt loading on the anode and cathode.[14] Bayer et al. reported a record high power density using sulfonated cellulose nanofibers using their spray coating technology.[44]

Even though higher power output was achieved, the procedure needed for reducing cellulose to nanocellulose is complex and expensive, while spray deposition is complex and still faces multiple fabrication challenges.[45] Gadim et al. reported an alternative approach by synthesizing membranes with 50 : 50 wt% blends of Nafion and bacterial cellulose which reported in-plane proton conductivity of 140 mS cm^{-1} at 90 °C and maximum power density of just 16 mW cm^{-2}.[46] In addition, chemically modified cellulose, which is primarily oxidized cellulose with a carboxylic group (–COOH) is employed in PEMFCs. Carboxylic acid, being hydrophilic in nature, is a strong charge carrier as it can accept and donate protons. Besides, due to the presence of stronger hydrogen bonds it has higher crosslinking which makes a denser, more mechanically robust nanopaper that can withstand high temperatures.[47] This type of PEMFC having a cellulose nanopaper membrane containing –COOH groups achieved a power density of 19.1 mW cm^{-2}.[13] However, the fabrication process is not facile and involves many steps.

Here we report on an alternative method, which uses a standard cellulose filter paper treated with weak acids and impregnated with resorcinol bis(diphenyl phosphate) (RDP),
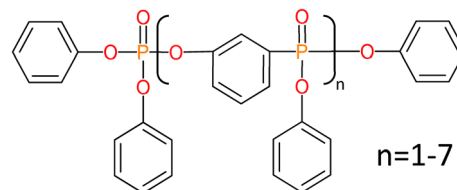

Fig. 1   Chemical structure of RDP.

which is a well-known flame retardant, and has been shown to hydrogen bond to cellulose enriching the fibers in PO$_3$–H functionalities. This method utilizes a simple procedure which is easy to implement producing high power output as compared to others reported in the literature (Fig. 1).[43]

2. Experimental

2.1 Chemicals and materials

The chemicals used in this study were of analytical purity and were employed without any additional purification. Ahlstrom, a company based in Helsinki, Finland, provided a cellulose filter paper (#610) with a diameter of 7.5 cm, thickness of 200 μm, and an average pore size of 1.5 μm. Carbon electrodes with 0.1 mg cm^{-2} Pt loading were procured from FuelCellsEtc, a company located in College Station, Texas. The RDP used in the experiment was obtained from ICL Industrial Products America, based in Tarrytown, NY. Citric acid monohydrate and phosphoric acid (85%) were obtained from Sigma-Aldrich. Additionally, Airgas in Radnor, PA provided the following gases with their respective purities: H$_2$ (99.999%), N$_2$ (99.9%), air (Dry, 20–22% O$_2$), and O$_2$ (99.8%).

2.2 Membrane fabrication

Cellulose filter papers were immersed in 100 mL of 1 Molarity solutions of citric acid (C$_6$H$_8$O$_7$), phosphoric acid (H$_3$PO$_4$) and a mixture of these two acids at 1 : 1 ratio (mixed acids), respectively, for 24 h, then membranes were washed in two separate aliquots of 500 mL distilled H$_2$O. All membranes were dried overnight at room temperature; then they were coated with RDP by dropping six drops of RDP on one side of the membrane and three drops of RDP on the other side using a plastic pipette and a pair of forceps. Plain cellulose filter paper was also prepared with RDP and used as a control. Membranes were then placed in an oven at 150 °C for 20 minutes to uniformly disperse the RDP across the membrane and dry the membrane.

2.3 Determination of the cellulose to RDP ratio and membrane thickness

The cellulose filter papers were initially weighed prior to immersion in RDP, then weighed again after drying and insertion into the MEA for testing. The thickness of different membranes was measured using a Vernier caliper (Tokyo, Japan).

The membranes prepared from the cellulose filter papers were characterized with respect to the amount of RDP by

Table 1 Weight of cellulose membranes

Membranes	Cellulose	Cellulose/RDP
Weight (mg)	388.6 ± 6	588.9 ± 4
Cellulose : RDP	n/a	2 : 1

weighing the membranes before and after drying them in the oven at 150 °C. The results are tabulated in Table 1 and represent the average of at least three membranes. From the table we can see that cellulose to RDP ratio is 2 for the membranes. This ratio was further confirmed using NMR. To investigate the ratio of cellulose : RDP and for a detailed peak assignment, we fitted the ^1H spectrum of cellulose with mixed acids/RDP by using DMFIT software (Fig. 7(a)). The RDP with full width at half maximum (FWHM) of 15–30 Hz and acid protons (with FWHM = 36–50 Hz) are well fitted with narrow peaks. The molecular structure of RDP and their peak assignments are shown in Fig. 7(a). Additional minor ^1H peaks could be due to the other negligible contribution of unknown components. The broad cellulose ^1H peak is simulated with single ^1H peak (FWHM = 1820 Hz). Based on the peak intensities of cellulose (20 H) and RDP (24 H), the estimated ratio of cellulose : RDP is 2 : 0.94, consistent with the experimentally measured ratio of 2 : 1. The thickness of the cellulose/RDP was measured to be 210 ± 2 μm, while it is 195 ± 3 μm for the pure cellulose filter.

2.4 Membrane characterization

Fourier transform infrared spectroscopy (FTIR) was performed using a PerkinElmer Frontier FT-IR spectrometer with an attenuated total reflection (ATR) accessory. Thirty-two scans were averaged to obtain each spectrum.

XRD measurements were performed employing an D8 Advance diffractometer (Bruker, USA) operating at 40 kV and 40 mA equipped with a copper target. XRD Patterns were collected over a 10–70 two-theta range with 0.01 step size and 1 s acquisition per step. Individual peaks were refined with pseudo-Voigt functions in TOPAS (Bruker, USA) with peak positions, widths and heights allowed to vary. The crystallinity of the membranes was calculated using $I_c = (I_{total} - I_{amor})/I_{total}$, where I_{total} is the intensity of the crystalline and amorphous parts (peak intensity of ~22.7°) and I_{amor} is the intensity of the amorphous part (the minimum position between the 002 and the 101 peaks) of the sample.

Full-field X-ray computed tomography data sets were collected for a series of specimens, employing a Zeiss Xradia 520 Versa X-ray microscope. The X-ray source was operated at 40.20 kV and 74.7 μA (3 W). The isotropic voxel size was set to 2.1 μm and a series of 1601 projections were collected over 360° with a 2.5 s image collection time per step. Data reconstruction was performed using a filtered-back projection algorithm. Data was visualized in ImageJ software.

The cellulose filter papers were applied onto Scanning electron microscopy (SEM) pin stubs using double side carbon tapes. They were then sputter-coated with gold to a thickness of 5 nm using a Leica EM ACE600 Coater for better electrical

conductivity. These samples were then imaged in a Thermo Scientific (FEI) Helios NanoLab 660 FIB-SEM with HT of 5 kV, current of 25 pA with ETD (Everhart-Thornley) detector. EDX (energy-dispersive X-ray spectroscopy) mapping was collected with an Oxford detector at HT of 10 kV and current of 1.6 nA. Data was collected and analyzed using AZtec software.

One-dimensional (1D) ^1H magic angle spinning (MAS) NMR spectra of cellulose fiber membranes were collected on a 300 MHz Varian NMR spectrometer operating at a magnetic field of 7 T equipped with 1.6 mm double resonance probe head. The sample was spun at 29 kHz MAS speed. The ^1H signal accumulated over 16–32 transients with at least 5 s recycling delay. 1D ^{13}C MAS and $^{13}C\{^1H\}$ CPMAS NMR spectra were collected on a 400 MHz NMR spectrometer operating at magnetic field of 9.4 T using a 4 mm double resonance probe head by spinning the sample at 10 kHz. The signal in ^{13}C MAS experiment was collected for 1k scans with 5 s recycling delay. In $^{13}C\{^1H\}$ CPMAS NMR, RAMP cross-polarization (CP) sequence was implemented to full fill the Hartmann-Hahn condition for efficient signal transfer. The contact pulse duration was set to 5 ms. The signal accumulated for 2k transients with 2 s recycling delay. The ^1H and ^{13}C chemical shifts were externally reference to a standard TMS. All NMR experiments were performed at room temperature.

2.5 Fuel cell testing

The evaluation of single cell performance was performed using a fuel cell test station obtained from Fuel Cell Technologies, Inc. A commercial carbon cloth gas diffusion layer electrode with a Pt loading of 0.1 mg cm^{-2} was utilized as both the anode and cathode. To assemble the membrane electrode assembly (MEA), the as-prepared cellulose filter membrane was placed between the electrodes, and uniform pressure was applied across the MEA. Testing was conducted with 99.99% pure H_2 flowing at 50 sccm at the anode and 100 sccm of air at the cathode. The gases at both the cathode and anode were humidified to 100% relative humidity (RH) and heated to 5 °C above the operating temperature to avoid condensation. The test was performed on an MEA with an active area of 5 cm^2 at four different temperatures (30 °C, 60 °C, 80 °C, and 90 °C).

To conduct the stability test of the cellulose/RDP membranes treated with mixed acids, the test station was operated at a constant current of 60 mA, corresponding to an initial voltage of 0.6 V. The voltage output was monitored continuously for 100 hours during constant operation.

2.6 Proton conductivity measurement

The proton conductivity of the membrane was measured by using an electrochemical impedance analyzer (Bio-Logic, SP200) directly connected to the cell. Prior to the measurement, H_2 and N_2 gases with a flow rate of 100 sccm and 100% relative humidity (RH) were flowed through the anode and cathode side of the membrane for 1 hour at 80 °C. The AC frequency was swept from 5 MHz to 1 Hz at a voltage amplitude of 5 mV. The proton conductivity (S cm^{-1}) was determined using the following formula:
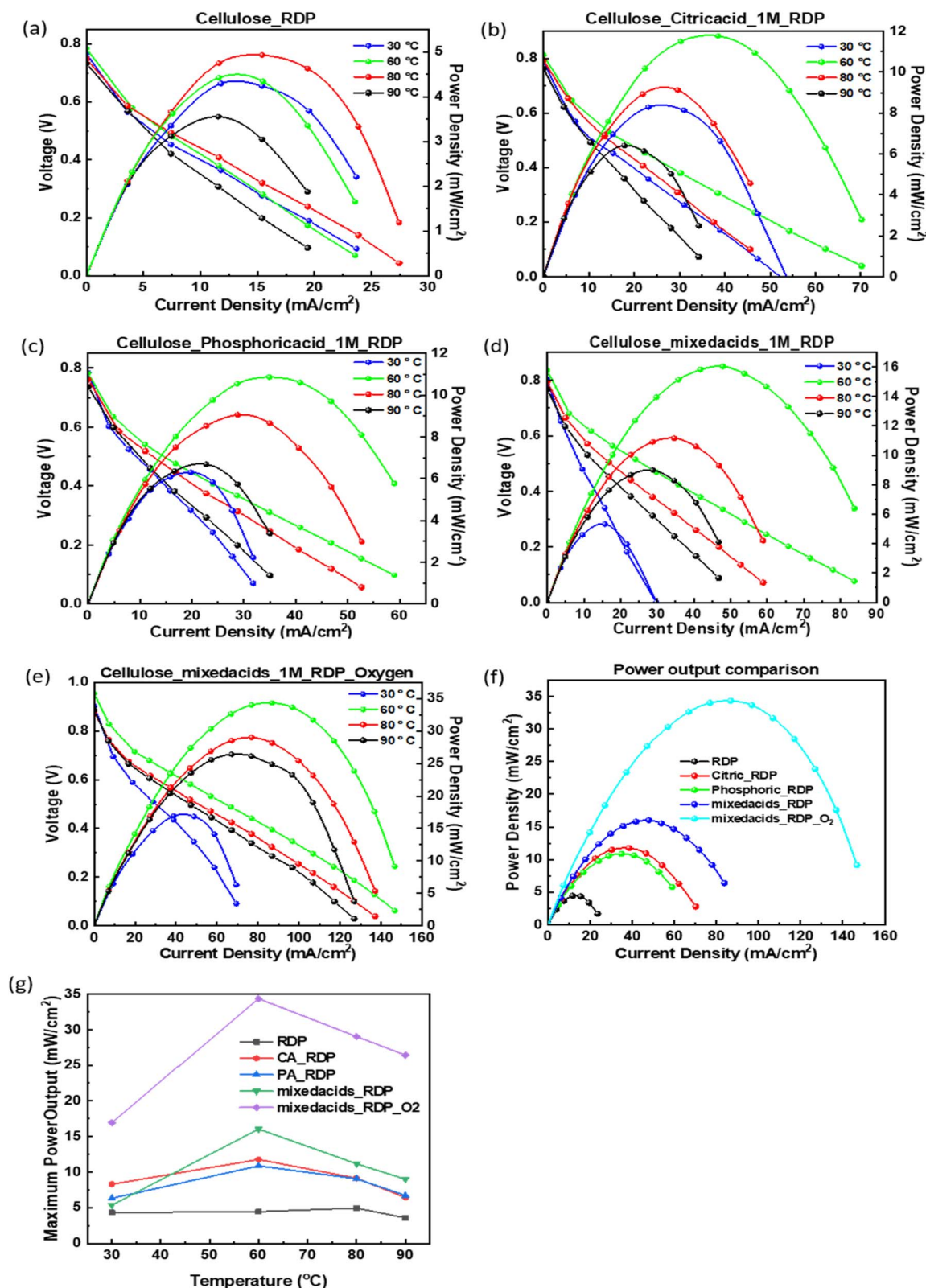
Fig. 2   Polarization curves for cellulose/RDP membrane with (a) no treatment (b) citric acid (c) phosphoric acid (d) mixed acids (e) mixed acids run in an oxygen environment (f) comparison of the max power performance for corresponding MEA (g) comparison of the power performance as a relation of temperature for each MEA.

$$\sigma = L \, (R \times A)$$

where L is the thickness of the membrane in cm, A is the cross-sectional area of the membrane in cm^2, and R represents the membrane resistance derived from the high frequency intercept in Ω.

2.7 Ion exchange capacity measurement

To determine the ion exchange capacity (IEC) of each membrane, 2 cm × 2 cm square pieces of the membranes were weighed before being soaked in 200 mL of 1 M H$_2$SO$_4$ solution for 24 hours. The membrane pieces were then washed thoroughly several times to remove excess acid. To replace protons with sodium ions, the samples were placed in 50 mL of 1 M NaCl solution and equilibrated at 40 °C for at least 24 hours. The remaining solution was titrated with 0.01 N NaOH solution using pH as the indicator, with the pH of 1 M NaCl solution measured using a pH meter (AB150, Accumet) serving as the standard. The IEC value (m$_{eq.}$ g^{-1}) was calculated using the following equation:

$$\text{IEC} = (V_{\text{NaOH}} \times N_{\text{NaOH}})/W_{\text{dry}}$$

where V_{NaOH} is the volume of NaOH used in the titration in mL, W_{dry} is the dry weight of the membrane in g, and N_{NaOH} is the normality of NaOH solution used for titration.

3. Results and discussion

3.1 Fuel cell test

The assembled membrane electrode assemblies (MEAs), incorporating the acid-treated and impregnated membranes, were tested in a fuel cell station, and the resulting polarization and power density curves are displayed in Fig. 2. From the power density results, it is evident that all RDP-containing membranes generated power across the temperature range of 30–90 °C. Fig. 2(f) shows the maximum power densities achieved for each membrane. Under atmospheric conditions, dipping cellulose in RDP yielded a maximum power output of 5 mW cm^{-2}. Adding

phosphoric acid more than doubled this output to 10.9 mW cm^{-2}, while citric acid slightly increased it to 11.8 mW cm^{-2}, suggesting that the pH, rather than the presence of phosphate alone, plays a key role in boosting performance. This is consistent with a recent review by Cui *et al.* which concluded that lowering the PH contributes to the enhancement of the HOR kinetics, due to the addition of proton conductors.[48] Notably, the combination of both acids resulted in a maximum power of 16.1 mW cm^{-2}, indicating a synergistic effect when both acids are present. For comparison, Songtao *et al.*[14] previously reported a maximum power of 27.7 mW cm^{-2} using carboxycellulose nanofibers (CNFs) cross-linked with citric acid and operated in an oxygen environment. When we tested this MEA under pure oxygen, as shown in Fig. 2(e), we observed a significantly higher maximum power of 34.3 mW cm^{-2}, despite the simpler processing method used in our study. In Fig. 2(g), the maximum power density for each membrane is plotted as a function of operating temperature. The membrane containing only RDP exhibited a relatively constant power output with a slight peak at 80 °C. In contrast, the acid-treated membranes displayed a pronounced power peak at 60 °C, particularly for the MEA tested in oxygen.

3.2 Proton conductivity measurements

We conducted further tests to investigate the proton conductivity, ion exchange capacity (IEC), and endurance of the acid-treated membranes. These properties are essential for evaluating the membranes' performance and potential application in proton exchange membrane fuel cells (PEMFCs). By examining these factors, we aimed to gain a comprehensive understanding of the acid-treated membranes' suitability for PEMFC use and their ability to enhance power generation efficiency. Ion exchange capacity (IEC) was measured according to the protocol which was described in the ref. 46. We found that the pH of the remaining solution of pure cellulose filter sample was similar to the original NaCl solution. For the cellulose/RDP sample, we obtained 0.04 m$_{eq.}$ g^{-1} IEC. With the citric acid treatment, the IEC increased to 0.07 m$_{eq.}$ g^{-1} and with the phosphoric acid treatment, the IEC
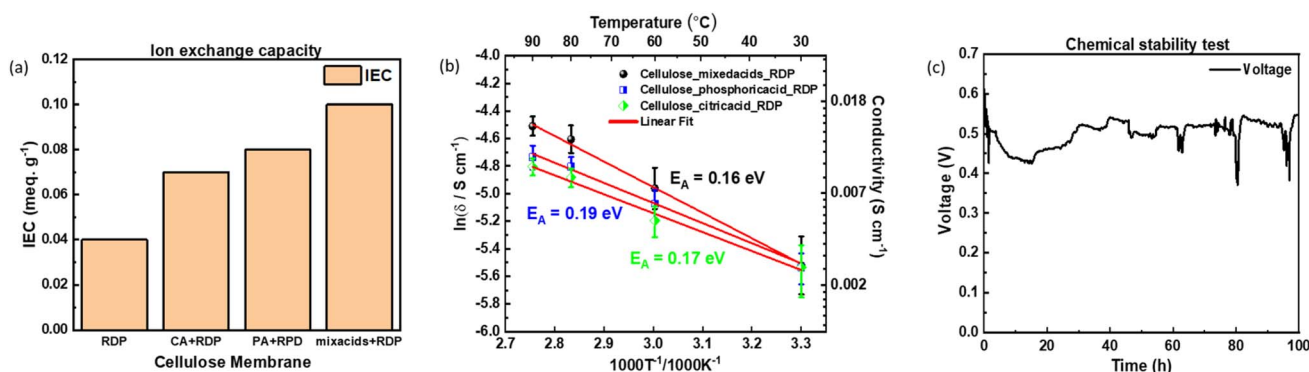

Fig. 3 (a) Ion exchange capacity of different treatment cellulose membranes. (b) Arrhenius curve of the proton conductivity of cellulose/RDP and mixed acids membranes with activation energy. The straight line is a linear fit to the Arrhenius model (error bars are for conductivity data points). (c) Voltage output of cellulose/RDP membrane treated with mixed acids under 60 mA constant current load at 60 °C for 100 hours continuous operation (sharp peaks occurred when gas cylinder changes).
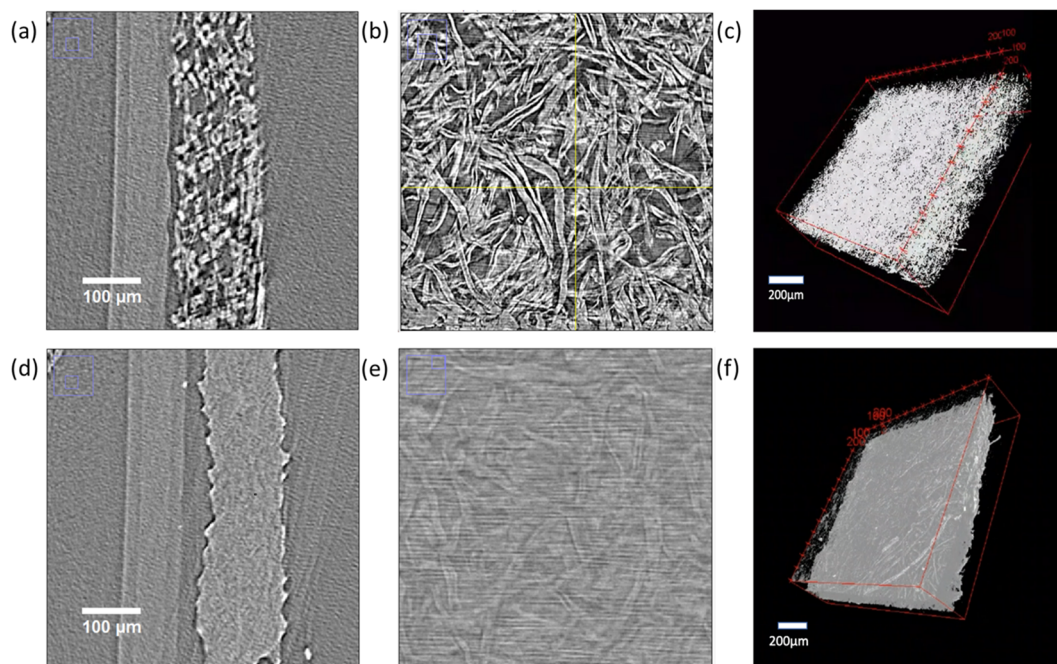
Fig. 4 Micro-CT images obtained in the (a) *XY*, (b) *XZ* planes and (c) 3D structure of the cellulose filter paper treated with mixed acids and (d) *XY*, (e) *XZ* and (f) 3D structure of the cellulose/RDP membrane treated with mixed acids.

increased to 0.08 $m_{eq.}\ g^{-1}$. The Cellulose filter paper membranes treated with mixed acids and RDP demonstrated the highest IEC with 0.1 $m_{eq.}\ g^{-1}$, which is in agreement with the power output demonstrated by each of the membranes (Fig. 3(a)).

Activation energy can be determined from the slopes of the Arrhenius plot and can provide valuable information about the possible proton conduction mechanism. Fig. 3(b) displays the Arrhenius plot of the conductivity of the membrane measured under different operating temperature conditions. As the temperature increased from 30 °C to 90 °C, the proton conductivity increased from 0.004 S cm^{-1} to 0.011 S cm^{-1} for the mixed acids treated cellulose/RDP membrane. The calculated activation energy of 0.16 eV (15.44 kJ mol^{-1}) is lower than the activation energy reported for Cellulose/RDP membrane treated with phosphoric acid (0.19 eV) and with citric acid (0.17 eV), which suggests that in addition to the proton hopping mechanism along the oxygen groups of cellulose, it is likely that the acid groups of citric and phosphoric acid contribute extra negatively charged sites to enhance the proton hopping and thus decrease the activation energy.[43,49–51]

In Fig. 3(c), we plot the MEA voltage as a function with time, when the cellulose cell was operated under constant current condition, which achieves an initial voltage of 0.6 V with 60 mA. In this figure, we can see that the voltage decreases by only 60 mV, from 0.60 V to 0.55 V, namely 8%, over a period of 100 hours for the mixed acids treated cellulose/RDP membrane. When we compare it to our previous research with cellulose/Nafion membrane which had a decrease from 0.6 to 0.54 V and cellulose/RDP membrane which had a decrease of 20% from 0.6 V to 0.48 V, the acid treated cellulose/RDP membranes have a good chemical stability comparable to cellulose/Nafion membrane.[11]

3.3 Characterization

To understand the robust power output that we are observing with the addition of RDP, the membranes were characterized by several complementary techniques.

3.3.1 Micro-CT and SEM/EDX. In a previous publication we showed that fabrication of PEM fuel cell membranes from citric acid cross linked nanocellulose required pressing at high pressure and temperature.[11] SEM imaging showed that this technique produced low porosity membranes, hence minimizing hydrogen gas cross-over and enabling power generation. Here we use unprocessed cellulose filter paper, which consists
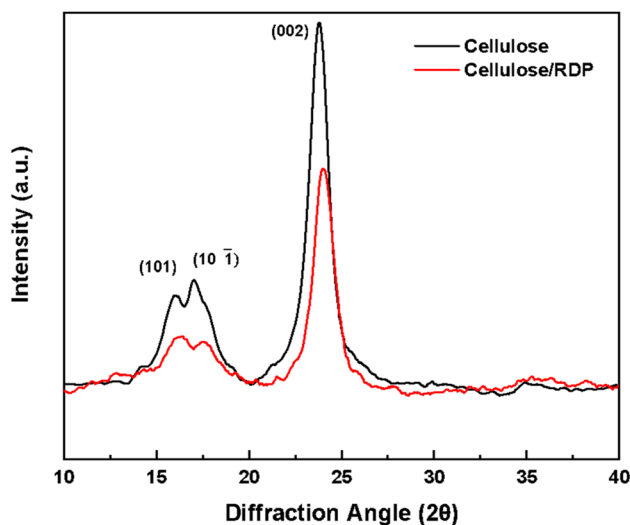

Fig. 5 XRD results of cellulose filter, cellulose/RDP membranes.

of a large cellulose fiber mesh, with 1.5 μm pore size. The hydrogen gas crossover through this type of membrane would be inconsistent with any power generation. We therefore examined the membranes first using micro-CT, in order to determine the pore structure in three dimensions. The data are shown in Fig. 4(a–c) where we show the micro-CT images from the micro-cellulose filter paper, both in front and side views.

From the figure we can see the porosity, as expected, is continuous throughout the filter paper. In Fig. 4(d–f) we show the micro-CT images of the RDP modified membranes, where we can clearly see that no porosity is apparent throughout the membrane. SEM and EDX microscopy were also performed in order to produce an elemental map across the membrane, which confirmed the presence of RDP. Secondary electron SEM
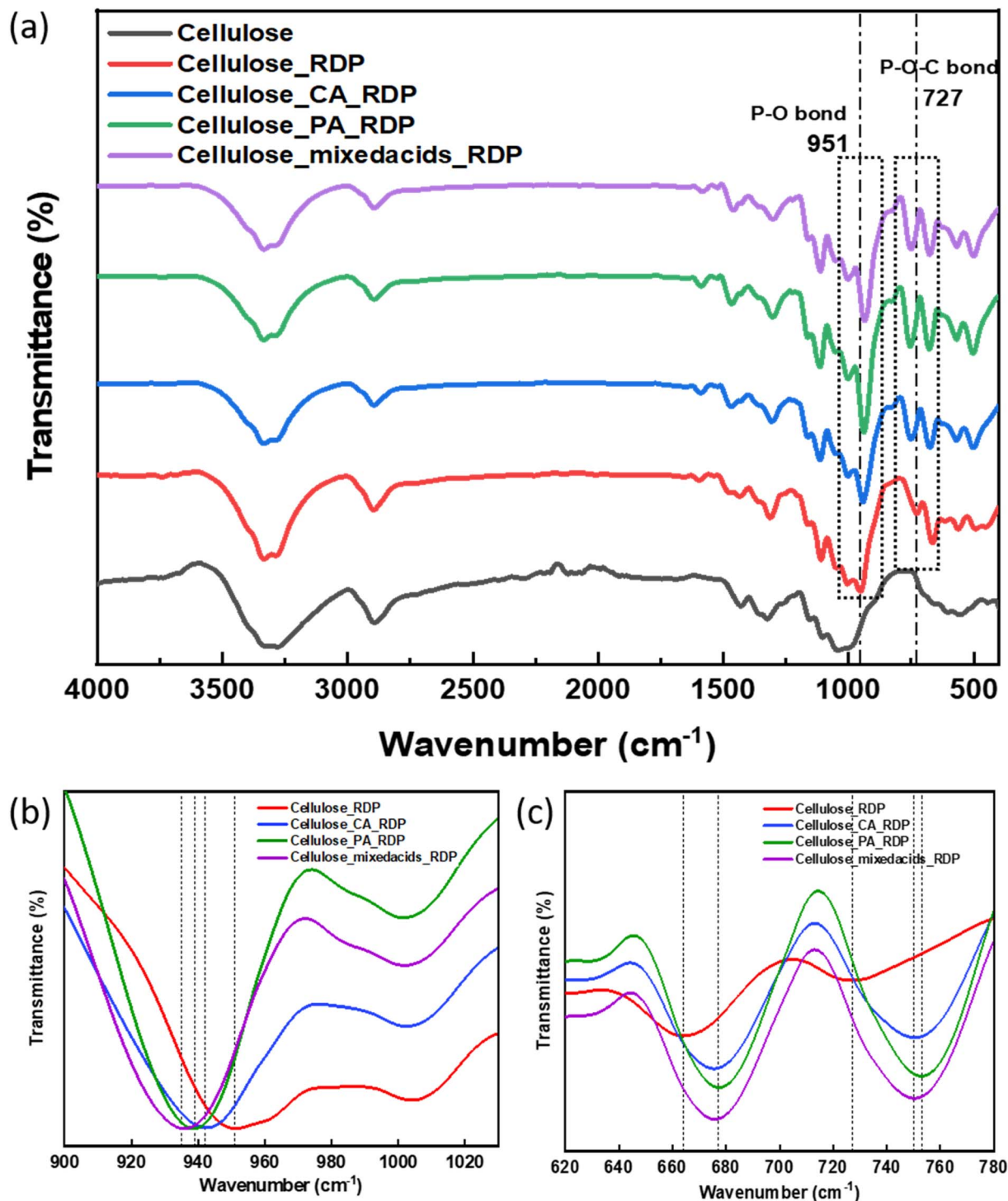

Fig. 6 (a) FTIR and (b and c) magnified dashed square region in (a) of the cellulose membrane, cellulose/RDP membrane and cellulose/RDP membrane treated with various acids.

images are shown in Fig. S3,† where we can see that a membrane like film had formed. EDX imaging showed distinct Phosphorus signals originating from RDP which appeared uniformly distributed across the membrane. The phosphorus signal was most prominent in the Cellulose/RDP membrane which was treated with either phosphoric acid alone or a mixture of citric and phosphoric acids.

3.3.2 XRD, FTIR. In Fig. 5 we compare the XRD spectra of the original filter paper membrane, where we obtain well defined peaks corresponding to a degree of crystallinity of 89.6%. Impregnating the paper with RDP is seen to reduce the crystallinity somewhat to 76.3% (Fig. S2†), but the peak position is unshifted indicating that RDP has penetrated into the cellulose structure and decreased the crystallinity, but did not change the basic crystal structure.

In contrast, the FTIR spectra plotted for all the MEAs in Fig. 6(a) show that multiple interactions have occurred. Initially, impregnating the cellulose with RDP we find a large downward energy shift from 687 cm^{-1} to 665 cm^{-1} corresponding to the C–H vibration of the benzene ring in pure RDP.[52] Another large downward shift in cellulose/RDP is seen at 757 cm^{-1} to 730 cm^{-1} which corresponds to the P–O–C bond vibration and

smaller changes are observed in the P–O bond, from 959 cm^{-1} to 951 cm^{-1}.[53] The FTIR component spectra corresponding to cellulose peaks can be seen at 3340 cm^{-1} and 2894 cm^{-1}, which corresponds to the O–H bending and C–H stretching, respectively. Addition of RDP does not change the position of the peak, but the FWHM of the peak at 3340 cm^{-1} becomes narrower, while the peak at 2894 cm^{-1} remains unchanged. Similarly, the C–H and the C–O segments remain unaffected by RDP. This indicates that initially the benzene ring of the phenol groups in RDP interacts mostly with the OH groups of the cellulose ring, stretching the entire P–O–C bond with very little bending of the P–O bond.

Treating the cellulose filter with acids, and then exposure to RDP, introduced multiple changes in the FTIR spectra, indicating a different form of interaction. The addition of acid decreased the intensity of peaks at 3340 cm^{-1} and 2894 cm^{-1} corresponding to the O–H bending and C–H stretching of the cellulose, when the ester bond was formed, making them unavailable to the RDP which is introduced after soaking in acid. Hence there was reduction of the energy shift at the P–O–C stretching and the benzene ring C–H binding sites. But, from Fig. 6(b) we find that the largest shift with RDP is now occurring
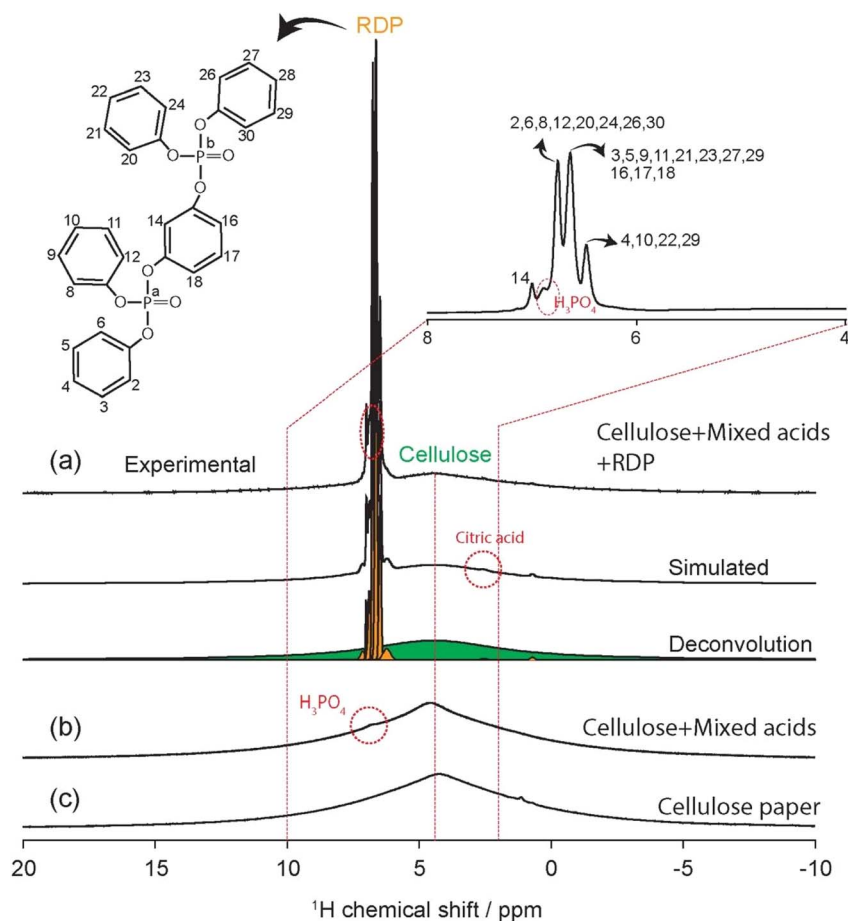

Fig. 7 (a–c) 1D ^{1}H MAS NMR spectra of cellulose filter paper (c), cellulose mixed acids without (b) and with RDP (a) collected on a 300 MHz spectrometer using 1.6 mm double resonance probe with 29 kHz MAS speed. The ^{1}H spectrum of cellulose mixed acids/RDP was deconvoluted to distinguish the signature of cellulose and RDP/acids protons (a). The molecular structure of RDP with ^{1}H peak assignments are shown in (a). ^{1}H peak at 6.9 ppm corresponding to H$_3$PO$_4$ is very significant in the case of cellulose mixed acids/RDP (a).

© 2025 The Author(s). Published by the Royal Society of Chemistry

at the P–O vibration, which shifted from 959 cm^{-1} to 942 cm^{-1} with citric acid, 939 cm^{-1} with phosphoric acid and to 935 cm^{-1} when a mixture of both acids is used indicating that a different binding site, namely the P–O bonding is involved where RDP binds to acid modified cellulose. This shift in binding location is further confirmed when we notice that the peaks at 1300 cm^{-1} and 570 cm^{-1}; and 1120 cm^{-1} corresponding to stretching of P=O double bond and C=O vibration are unaffected.

3.3.3 **^{1}H MAS NMR.** As shown in Fig. 7, ^{1}H and ^{13}C MAS NMR spectra were collected to establish the structural and dynamical insights of studied cellulose materials. The ^{1}H spectrum of cellulose paper (Fig. 7(c)) that displays a broad ^{1}H peak centered at 4.5 ppm could be assigned to the protons of cellulose structural units. ^{1}H NMR spectrum of cellulose with mixed acids (Fig. 7(b)) also shows a broad peak corresponding to the cellulose protons. A small peak at 6.8 ppm could be assigned to the H$_3$PO$_4$. A slight downfield shift of this ^{1}H peak as compared to 85% H$_3$PO$_4$ (5.7 ppm) suggests that the acid groups may form strong H-bonds with cellulose functional groups, consistent with the FTIR. On the other hand, ^{1}H features of citric acid are not evident in the ^{1}H NMR spectrum, which may be hidden under the broad cellulose ^{1}H peak. This could be mainly due to the slow mobility of protons. However, in the case of cellulose with mixed acids and RDP (Fig. 7(a)), narrow ^{1}H peaks corresponding to H$_3$PO$_4$ (6.9 ppm) and citric acid (2.6 ppm) can be clearly distinguished from the broad cellulose ^{1}H peak centered at 4.5 ppm, in addition to four narrow ^{1}H peaks of RDP in the aromatic region. In particular, the ^{1}H peak at 6.9 ppm (H$_3$PO$_4$), which is small and broad for cellulose mixed acids without RDP, becomes narrow and intense for the one with RDP. This highlights the fact that RDP in cellulose paper significantly improves the proton dynamics of acid groups, which explains the decreased activation energy shown in Fig. 3(b) and the increase in power output for the Cellulose/mixedacids/RDP membrane.

4. Conclusion

To summarize, this investigation aimed to develop a new type of membrane for PEM fuel cells by treating cellulose-filter paper with weak acids and reinforcing it with RDP in a 2 : 1 ratio. The results showed that the addition of RDP to the filter paper produced a film spanning between the cellulose fiber supports, which prevented gas crossover, while it also improved the proton dynamics of acid groups. FTIR spectra of the MEAs showed that while RDP was bound *via* the phenolic group to the OH groups in cellulose, addition of either citric, phosphoric, or a combination of both hydrolyzed the cellulose, causing RDP to bind *via* the P–O site. NMR analysis confirmed the strong hydrogen bonding of RDP to untreated cellulose which decreased proton mobility. Strong binding of acids to cellulose also resulted in slow proton mobility, but the addition of RDP, after acid treatment significantly enhanced the proton mobility, which is an important factor in power generation, and may account for the observed synergy and enhancement in power generation. Testing MEAs operated in atmosphere, with

membranes formed from cellulose filter paper, treated with RDP achieved a maximum power output of 4.9 mW cm^{-2} at 80 °C with only 0.1 mg cm^{-2} of platinum group metal (PGM) loading at the anode and cathode. Treatment with citric acid and phosphoric acid separately further enhanced the power output by 141% and 120% respectively, reaching a peak at 60 °C. The highest power was achieved with the MEA where the cellulose filter paper was first treated with a mixture of phosphoric and citric acids, and RDP, demonstrating the highest ion exchange capacity of 0.1 m$_{eq.}$ g^{-1} and an enhancement of 226% in power output, reaching 16 mW cm^{-2} in air and 34.3 mW cm^{-2} in oxygen environment. Furthermore, this membrane was stable under constant current of 60 mA, for at least 100 hours with only an 8% loss in voltage. This work shows that cellulose filter paper, which is an inexpensive, renewable, and sustainable material, can provide a potential alternative to traditional PEMFC membranes made from Nafion for low power applications.

Data availability

All relevant data are within the manuscript and its additional files.

Author contributions

Aniket Raut: data curation, formal analysis, investigation, methodology, validation, writing – original draft. Haoyan Fang: formal analysis, investigation, validation. Yu-Chung Lin: formal analysis, methodology. Md Farabi Rahman: formal analysis, investigation. Shi Fu: methodology. Yifan Yin: formal analysis, methodology. Yiwei Fang: formal analysis, software. David Sprouster: formal analysis, methodology, software. Rebecca Isseroff: resources, methodology, investigation. Sunil Sharma: methodology. Priyanka Sharma: methodology. Devanshi Bhardwaj: methodology. Mounesha N. Garaga: resources, formal analysis. Steve Greenbaum: formal analysis, resources. Sheng Zhang: formal analysis, resources. Miriam H. Rafailovich: conceptualization, formal analysis, supervision, writing – review & editing.

Conflicts of interest

There are no conflicts to declare.

Acknowledgements

References

1 K. K. Jaiswal, *et al.*, Renewable and sustainable clean energy development and impact on social, economic, and environmental health, *Energy Nexus*, 2022, 100118.

2 J. K. Mannekote, *et al.*, Environmentally friendly functional fluids from renewable and sustainable sources-A review, *Renewable Sustainable Energy Rev.*, 2018, **81**, 1787–1801.

3 L. Cui, *et al.*, Exploring the role of renewable energy, urbanization and structural change for environmental sustainability: Comparative analysis for practical implications, *Renewable Energy*, 2022, **184**, 215–224.

4 M. Saleem, Possibility of utilizing agriculture biomass as a renewable and sustainable future energy source, *Heliyon*, 2022, e08905.

5 E. Cuce, D. Harjunowibowo and P. M. Cuce, Renewable and sustainable energy saving strategies for greenhouse systems: A comprehensive review, *Renewable Sustainable Energy Rev.*, 2016, **64**, 34–59.

6 J. Qu, *et al.*, Doping by design: finding new n-type dopable ABX 4 Zintl phases for thermoelectrics, *J. Mater. Chem. A*, 2020, **8**(47), 25306–25315.

7 J. Li, *et al.*, X-ray Absorption Spectroscopy Studies of a Molecular CO_2-Reduction Catalyst Deposited on Graphitic Carbon Nitride, *J. Phys. Chem. C*, 2023, **127**(7), 3626–3633.

8 P. Huang, *et al.*, Revealing the structure of single cobalt sites in carbon nitride for photocatalytic CO2 reduction, *J. Phys. Chem. C*, 2022, **126**(20), 8596–8604.

9 J. Qu, *et al.*, Computational design of thermoelectric alloys through optimization of transport and dopability, *Mater. Horiz.*, 2022, **9**(2), 720–730.

10 P. Huang, *et al.*, Effect of Carbon Doping on CO_2-Reduction Activity of Single Cobalt Sites in Graphitic Carbon Nitride, *ChemNanoMat*, 2021, **7**(9), 1051–1056.

11 L. Wang, *et al.*, Operation of proton exchange membrane (PEM) fuel cells using natural cellulose fiber membranes, *Sustainable Energy Fuels*, 2019, **3**(10), 2725–2732.

12 L. Wang, *et al.*, Enhancing proton exchange membrane fuel cell performance via graphene oxide surface synergy, *Appl. Energy*, 2020, **261**, 114277.

13 S. K. Sharma, *et al.*, Nitro-oxidized carboxylated cellulose nanofiber based nanopapers and their PEM fuel cell performance, *Sustainable Energy Fuels*, 2022, **6**(15), 3669–3680.

14 S. Li, *et al.*, Sustainable Plant-Based Biopolymer Membranes for PEM Fuel Cells, *Int. J. Mol. Sci.*, 2022, **23**(23), 15245.

15 A. Raut, *et al.*, Effect of membrane mechanics on AEM fuel cell performance, *Energy Adv.*, 2023, **2**(1), 113–122.

16 J. Calderon, *et al.*, Power Enhancement of Anion Exchange Membrane Fuel Cells (AEMFCs) Through Spray-Coating of Membrane With Partially Reduced Graphene Oxide, *J. Undergrad. Chem. Eng. Res.*, 2022, 75–82.

17 T. Yingnakorn, *et al.*, Catalyst coated membranes for fuel cell and water electrolyser delamination induced by organic solution soaking and water ultrasonication, *RSC Sustainability*, 2025, **3**(4), 1900–1908.

18 T. Yingnakorn, *et al.*, Fast delamination of fuel cell Catalyst-Coated membranes using High-Intensity ultrasonication, *Ultrason. Sonochem.*, 2025, 107330.

19 K. Jiao, *et al.*, Designing the next generation of proton-exchange membrane fuel cells, *Nature*, 2021, **595**(7867), 361–369.

20 E. Ogungbemi, *et al.*, Selection of proton exchange membrane fuel cell for transportation, *Int. J. Hydrogen Energy*, 2021, **46**(59), 30625–30640.

21 H.-W. Wu, A review of recent development: Transport and performance modeling of PEM fuel cells, *Appl. Energy*, 2016, **165**, 81–106.

22 M. T. Gencoglu and Z. Ural, Design of a PEM fuel cell system for residential application, *Int. J. Hydrogen Energy*, 2009, **34**(12), 5242–5248.

23 A. Alaswad, *et al.*, Developments in fuel cell technologies in the transport sector, *Int. J. Hydrogen Energy*, 2016, **41**(37), 16499–16508.

24 J. Amphlett, *et al.*, A practical PEM fuel cell model for simulating vehicle power sources, in *Proceedings of the Tenth Annual Battery Conference on Applications and Advances*, IEEE, 1995.

25 Y. Wang, *et al.*, A review of polymer electrolyte membrane fuel cells: Technology, applications, and needs on fundamental research, *Appl. Energy*, 2011, **88**(4), 981–1007.

26 E. Zhu, *et al.*, Stability of Platinum-Group-Metal-Based Electrocatalysts in Proton Exchange Membrane Fuel Cells, *Adv. Funct. Mater.*, 2022, **32**(30), 2203883.

27 K. E. Ayers, *et al.*, Pathways to ultra-low platinum group metal catalyst loading in proton exchange membrane electrolyzers, *Catal. Today*, 2016, **262**, 121–132.

28 L. Du, *et al.*, Low-PGM and PGM-free catalysts for proton exchange membrane fuel cells: stability challenges and material solutions, *Adv. Mater.*, 2021, **33**(6), 1908232.

29 W. Kiciński, *et al.*, Platinum group metal-free Fe– N– C catalysts for PEM fuel cells derived from nitrogen and sulfur doped synthetic polymers, *Fuel*, 2022, **328**, 125323.

30 Q. Meyer, *et al.*, Operando detection of oxygen reduction reaction kinetics of Fe–N–C catalysts in proton exchange membrane fuel cells, *J. Power Sources*, 2022, **533**, 231058.

31 A. Mehmood, *et al.*, High loading of single atomic iron sites in Fe–NC oxygen reduction catalysts for proton exchange membrane fuel cells, *Nat. Catal.*, 2022, **5**(4), 311–323.

32 S. Wang, A. Lu and L. Zhang, Recent advances in regenerated cellulose materials, *Prog. Polym. Sci.*, 2016, **53**, 169–206.

33 P. R. Sharma, *et al.*, A simple approach to prepare carboxycellulose nanofibers from untreated biomass, *Biomacromolecules*, 2017, **18**(8), 2333–2342.

34 P. R. Sharma, *et al.*, Nanocellulose from spinifex as an effective adsorbent to remove cadmium (II) from water, *ACS Sustain. Chem. Eng.*, 2018, **6**(3), 3279–3290.

35 P. R. Sharma, *et al.*, High aspect ratio carboxycellulose nanofibers prepared by nitro-oxidation method and their nanopaper properties, *ACS Appl. Nano Mater.*, 2018, **1**(8), 3969–3980.

36 T. Heinze, Cellulose: structure and properties, *Cellulose chemistry and properties: fibers, nanocelluloses and advanced materials*, 2016, pp. 1–52.

37 D. Klemm, *et al.*, Cellulose: fascinating biopolymer and sustainable raw material, *Angew. Chem., Int. Ed.*, 2005, **44**(22), 3358–3393.

38 L. J. Gibson, The hierarchical structure and mechanics of plant materials, *J. R. Soc. Interface*, 2012, **9**(76), 2749–2766.

39 I. Smolarkiewicz, *et al.*, Proton-conducting microcrystalline cellulose doped with imidazole. Thermal and electrical properties, *Electrochim. Acta*, 2015, **155**, 38–44.

40 L. Yue, *et al.*, Sulfonated bacterial cellulose/polyaniline composite membrane for use as gel polymer electrolyte, *Compos. Sci. Technol.*, 2017, **145**, 122–131.

41 J. A. Seo, *et al.*, Preparation and characterization of crosslinked cellulose/sulfosuccinic acid membranes as proton conducting electrolytes, *Ionics*, 2009, **15**, 555–560.

42 S. Thangarasu, *et al.*, Recent developments on bioinspired cellulose containing polymer nanocomposite cation and anion exchange membranes for fuel cells (PEMFC and AFC), *Polymers*, 2022, **14**(23), 5248.

43 T. Bayer, *et al.*, High temperature proton conduction in nanocellulose membranes: paper fuel cells, *Chem. Mater.*, 2016, **28**(13), 4805–4814.

44 T. Bayer, *et al.*, Spray deposition of sulfonated cellulose nanofibers as electrolyte membranes in fuel cells, *Cellulose*, 2021, **28**, 1355–1367.

45 A. Karaca, *et al.*, Self-Standing, Ultrasonic Spray-Deposited Membranes for Fuel Cells, *Membranes*, 2023, **13**(5), 522–553.

46 T. D. Gadim, *et al.*, Nafion® and nanocellulose: A partnership for greener polymer electrolyte membranes, *Ind. Crops Prod.*, 2016, **93**, 212–218.

47 A. L. Chibac-Scutaru, *et al.*, Advances in the use of cellulose-based proton exchange membranes in fuel cell technology: A review, *Int. J. Biol. Macromol.*, 2023, **247**, 125810.

48 W.-G. Cui, *et al.*, Insights into the pH effect on hydrogen electrocatalysis, *Chem. Soc. Rev.*, 2024, **53**, 10253.

49 P. Kumar, *et al.*, Membrane prepared by incorporation of crosslinked sulfonated polystyrene in the blend of PVdF-co-HFP/Nafion: a preliminary evaluation for application in DMFC, *Appl. Energy*, 2014, **123**, 66–74.

50 M. Eikerling, *et al.*, Mechanisms of proton conductance in polymer electrolyte membranes, *J. Phys. Chem. B*, 2001, **105**(17), 3646–3662.

51 G. A. Luduena, T. D. Kühne and D. Sebastiani, Mixed Grotthuss and vehicle transport mechanism in proton conducting polymers from ab initio molecular dynamics simulations, *Chem. Mater.*, 2011, **23**(6), 1424–1429.

52 A. Shigematsu, T. Yamada and H. Kitagawa, Wide control of proton conductivity in porous coordination polymers, *J. Am. Chem. Soc.*, 2011, **133**(7), 2034–2036.

53 Y.-M. Jang, *et al.*, Preparation and flame retardant properties of cotton fabrics treated with resorcinol bis(diphenyl phosphate), *Cellulose*, 2021, **28**, 4455–4467.